A Highly Miniaturized Wireless Inertial Sensor using a Novel 3D Flexible Circuit

J. Buckley, B. O'Flynn, J. Barton, A. Murphy, S.C. O'Mathuna

Tyndall National Institute, Lee Maltings, Prospect Row, Cork, Rep. Ireland.

ABSTRACT

Purpose

To develop a highly miniaturized wireless inertial sensor system based on a novel 3D packaging technique using a flexible printed circuit. The device is very suitable for wearable applications in which small size and light weight are required such as body area networks for medical, sports and entertainment applications.

Design/methodology/approach

Modern wireless inertial measurement units are typically implemented on a rigid 2D printed circuit board (PCB). The design concept presented here is based around the use of a novel planar, 6-faceted, crucifix or cross-shaped flexible printed circuit (FPC) instead of a rigid PCB. A number of specific functional blocks (such as MEMs gyroscope and accelerometer sensors, microcontroller (MCU), radio transceiver, antenna etc) are first assigned to each of the 6 faces which are each 1cm squared in area. The FPC cross is then developed into a 1cm cubed, 3D configuration by folding the cross at each of 5 bend planes. The result is a low-volume and lightweight, 1.5 cm cubed wireless inertial sensor that can sense and send motion sensed data wirelessly to a base station. The wireless sensor device has been designed for low power operation both at the hardware and software levels. At the base station side, a radio receiver is connected to another MCU unit, which sends received data to a PC and

graphical user interface (GUI). The Industrial, Scientific and Medical (ISM) band (2.45GHz) was used to achieve half duplex communication between the two sides.

Findings

A complete wireless sensor system has been realized in a 3D cube form factor using a flexible printed circuit. The packaging technique employed during the work was shown to be efficient in fabricating the final cubic system and resulted in a significant saving in the final size and weight of the system. A number of design issues were identified regarding the use of flexible printed circuit for implementing the 3D structure and the chosen solutions were shown to be successful in dealing with these issues.

Research limitations/implications

Currently, a limitation of the system is the need for an external battery to power the sensor system. A second phase of development would be required to investigate the possibility of the integration of a battery and charging system within the cube structure. In addition, the use of flexible substrate imposes a number of restrictions in terms of the ease of manufacturability of the final system due to the requirement of the required folding step.

Practical implications

The small size and weight of the developed system was found to be extremely useful in different deployments. It would be useful to further explore the system performance in different application scenarios such as wearable motion tracking applications. In terms of manufacturability, component placement needs to be carefully considered, ensuring that there is sufficient distance between the

components, bend planes and board edges and this leads to a slightly reduced usable area on the printed circuit.

Originality/value

This paper provides a novel and useful method for realizing a wireless inertial sensor system in a 3D package. The value of the chosen approach is that a significant reduction in the required system volume is achieved. In particular, a 78.5% saving in volume was obtained in decreasing the module size from a 25mm to a 15mm cubed size.

Keywords: Wireless sensor networks, low power, flexible printed circuit, medical and body area network applications.

INTRODUCTION

This paper introduces a highly miniaturized, 6-degree-of-freedom (DOF) wireless inertial sensor that can be used when a small, light-weight, low-power design is required for size-sensitive applications such as wearable, wireless sensor systems. Electromechanical inertial sensors have been used for guidance, navigation and control applications since the emergence of inertial sensing in the early 1920s [1]. In recent years, these sensors have been implemented using Microelectromechanical Systems (MEMS) technology. MEMS technology has resulted in much smaller, low-cost inertial measurement devices being available on the market with increased reliability, lower production cost, high precision, wide dynamic range and small size. Compared to conventional inertial sensors, MEMS sensors have a smaller number of moving mechanical parts that ultimately gives rise to inherent robustness and durability [2].

The emergence of accurate, low cost miniaturized MEMS inertial sensors motivates the design of miniature inertial measurement units (IMU) for applications well outside the field of inertial navigation. For example, a recent application concerns novel sports training systems with inertial sensors embedded directly in sports equipment [3]. Other recent applications include wearable Wireless Body Area Sensor Networks (WBASN) for posture and activity recognition applications [4-5] and multimedia applications for an interactive dance environment [6], where this technology can be applied to the design of human-computer interfaces (HCI).

A number of 6 DOF miniaturized inertial sensors are described in the literature of late. A diminutive (size 30mm × 20mm × 10mm) inertial sensor has recently been described in [7-8] for cancer research applications that is capable of measuring position and orientation about three orthogonal axes for tumour motion tracking. It

has to be mentioned that this system only has two-axis gyroscope which makes it unsuitable for 6 DOF applications. Another miniaturized wireless inertial sensor has been presented in [9] that describes a system consisting of a number of miniature wireless inertial sensors that are attached to a person's limbs. The system communicates with a PC via a wireless receiver that interprets and presents the measurement data. Each of the sensors measures 3D acceleration, 3D-magnetization (earth magnetic field) and 3D angular velocity. This device however is matchbox sized and is quite large for wearable applications for example.

In terms of commercial sensor systems, there are a large number of 6 DOF commercial wireless inertial sensors on the market: A 2.45GHz wireless inertial measurement unit is available from [10] with a size of 58 × 43 × 26 mm. Another 6 DOF IMU is available from [11], enabling accurate orientation tracking. It provides drift-free 3D orientation as well as kinematic data including 3D acceleration, 3D rate of turn and 3D earth-magnetic field data. However this is a wired rather than a wireless system and the size is 38 × 53 × 51mm. The main problems with the above commercial devices are that they are all quite large and tend to be expensive. These devices are also difficult to customize and are power hungry.

A miniaturized wireless inertial sensor system has been developed in [12-14] as shown in Figure 1. This system employs a commercial, tri-axial MEMS accelerometer, three mutually orthogonal MEMS gyroscopes and three magnetometers to achieve full 6 DOF operation.

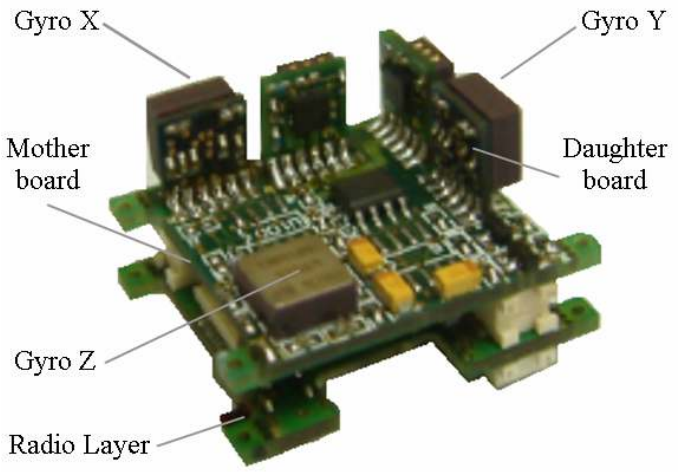

Figure. 1: 25mm Wireless Inertial Measurement Unit.

This IMU sensor works as part of a 25mm wireless sensor node platform [14]. It can be seen that gyroscope orthogonality is achieved using small daughter card PCBs mounted orthogonally to the main motherboard. The motherboard area is approximately 25mm squared. This IMU layer also features a tri-axial accelerometer as well as 3 magnetometers. The goal of this work is to drastically decrease the size of the above system and implement a fully wireless, 6 DOF wireless IMU (or WIMU). The feasibility of 3D packaging is evaluated based on the use of a flexible printed circuit (or flex) substrate that incorporates low-cost single-axis gyroscopes (as tri-axial gyroscopes not available at time of writing).

The paper is organised as follows. The first section deals with the design of the inertial sensor system. It presents detailed information on the functional blocks required for the system and concentrates on the design, implementation and manufacturing issues experienced with the use of a flexible interconnect substrate. The application development using the developed WIMU is then described in the next section. The key results are discussed in detail throughout the above two sections and conclusions are drawn in the final section.

SYSTEM DESIGN

A. System overview

Figure 2 illustrates the most basic method in remotely capturing motion data and transmitting it to a receiver or base station.

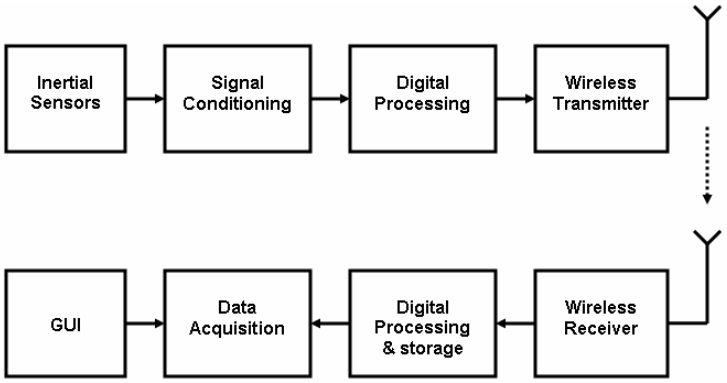

Figure. 2: Wireless Inertial Sensing System Block Diagram.

Inertial sensors (e.g. accelerometers, gyroscopes and magnetometers) sense movement and the sensor outputs (assuming analog outputs) are applied to a signal conditioning block. The signal conditioning stage usually has some form of amplification and filtering that are required to increase the amplitude and band-limit the sensor output signals prior to analog-to-digital conversion. In modern systems, an analogue-to-digital (A/D) conversion is carried out as soon as possible, to take advantage of the many possibilities that are offered by the ever-increasing power of digital electronics.

The transmitter stage sends the acquired and processed data to a remote receiver. At the receiver side, the signal is decoded, processed and the information of interest is made available to the user in a graphical user interface for example.

In order to implement the wireless inertial sensing system, a number of functional blocks are required as shown in Figure 3.

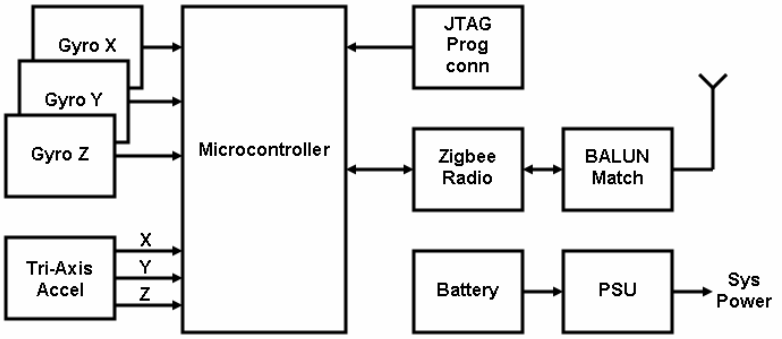

Figure. 3: Wireless Inertial Measurement System Architecture.

At the inception of this project, only single-axis gyroscopes were commercially available and therefore three gyros are required to provide the required 3 degrees of freedom. The analog output voltages need to be digitized and therefore a convenient and space saving method is to use a microcontroller with on-board ADC. A programming connector is required to allow the user program to be downloaded to the microcontroller. A radio IC and antenna are also required to wirelessly transfer the captured motion data to another receiver node or base station. A battery and power subsystem is required to provide system power.

Apart from the obvious small size requirement of the WIMU cubed system, a very important aspect of the design is to ensure low-power operation. To facilitate this requirement, each sub-system element needs to use as little power as possible during operation as well as in standby/sleep mode. MEMS gyroscopes in particular are power hungry devices and having the ability to enable or disable the power to the gyroscopes is something that is desirable.

B. 3D Package Implementation

In order to realize a 3D cubed system, a number of different packaging strategies were considered. In particular, the use of a flex material was chosen as the focus of this work. The chosen concept is to fold a 6-face crucifix shaped flexible printed circuit

into a cube as shown in Figure 4. A functional system block is assigned to each face, with the flexible PCB providing the means of interconnecting each of these faces.

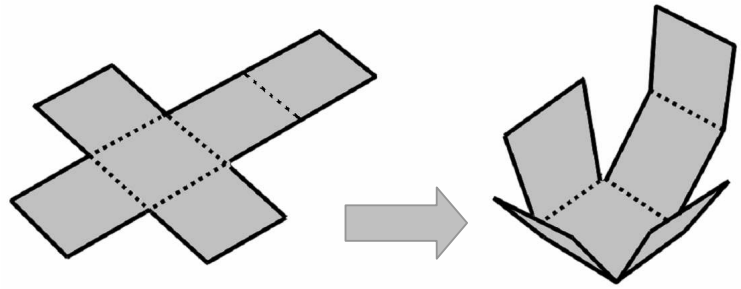

Figure. 4: Evolution of 2D to 3D cube structure.

For this system, each face of the crucifix is 10mm squared and the total size is 40mm × 30mm in length. The outer and inner layers of each are then assigned a specific function as shown in Figure 5.

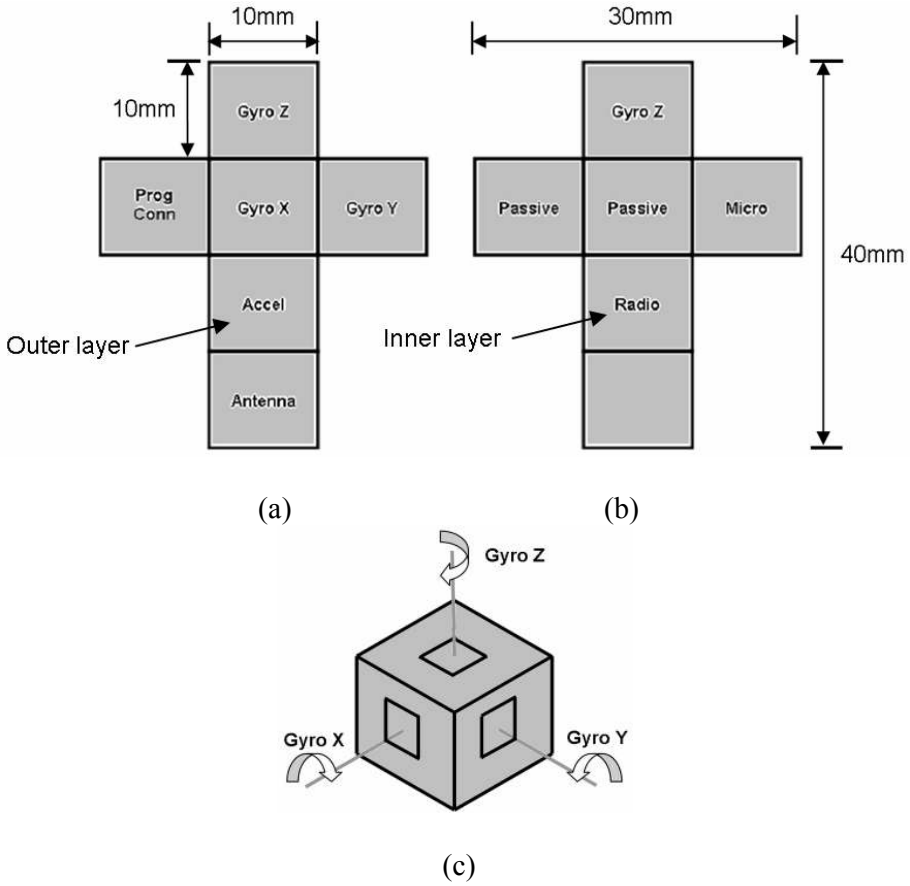

Figure. 5: Cube face functions, (a) Outer layer, (b) Inner layer, (c) Folded configuration

The assignment of functions to faces was chosen as follows: Single-axis gyros are mounted on three adjacent faces as shown in Figure 5(a) such that when folded, they are mutually orthogonal. A tri-axial accelerometer is mounted on an adjacent face. The radio transceiver IC and antenna are placed on adjacent faces to minimize RF losses between transceiver and antenna. In addition, when the device is folded, the antenna is placed on the outside surface of the cube to maximize the efficiency of the antenna. The surface behind the antenna is deliberately kept free of components so as not to adversely affect the antenna impedance and radiation characteristics. The microcontroller is assigned to another face and in order to conveniently program the device, a programming connector is assigned to the same face but on the outside layer to allow the microcontroller to be programmed without having to open the folded cube. The majority of discrete passive components such as capacitors, inductors and resistors are placed in the centre face, close to the four adjacent faces, easing the routability of the interconnect.

C. Sensor System Components

Having defined the functional blocks for the system and the manner in which these blocks have been partitioned on the substrate, the choice of components used to implement the system are now described in detail.

The chosen gyroscope for this application was the ADXRS150 ±150°/s MEMs angular rate sensor with on-chip signal conditioning [17]. The device has a package size of 7 × 7 × 3mm and allows the gyroscopes to fit comfortably in the centre of each of the three 10mm square cube faces on the flexible substrate. The gyro output signal, RATEOUT, is a voltage proportional to the angular rate about the axis normal to the top surface of the package as shown in Figure 6.

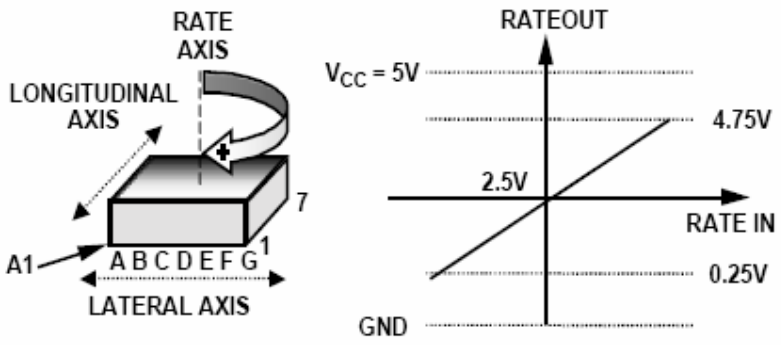

Figure. 6: RATEOUT Signal Increases with Clockwise Rotation [16].

A single-pole low-pass filter, consisting of an internal 9 kΩ resistor and an external user-supplied capacitor is used to filter the output data and sets the pass bandwidth of the RATEOUT signal. Since these gyros are single axis devices, three devices are required to provide angular rate sensing in three planes X, Y and Z as illustrated in Figure 5(c).

The accelerometer chosen for this application was the KXM52 device from Kionix [18]. This is a high-performance tri-axial sensor that consists of a sensor element and an ASIC packaged in a 5 × 5 × 1.8mm package. The sensor element functions on the principle of differential capacitance, with device acceleration causing the displacement of an internal silicon structure resulting in a change in capacitance. The sensitivity of the device is factory programmable allowing customisation for applications requiring ±1.0g to ±6.0g ranges and for this application, the ±1.0g device was chosen. As with the ADXRS150 gyroscope, the sensor bandwidth is user-definable by selecting the value of the output filter capacitors.

The chosen microcontroller was the ATMega128L device from Atmel [19]. This device is a high-performance, low-power AVR® 8-bit Microcontroller with an advanced RISC architecture with 53 programmable IO lines contained in a 64-pin 10 × 10 × 10 mm TQFP package. The device also provides 8 × 10-bit ADC channels that

are used for sensing the gyroscope and accelerometer signals. Some other features that are used in this application are the power-on reset and programmable brownout detection capabilities as well as an internally calibrated RC oscillator. Also critical to low power operation are the sleep mode, power-save, power-down and standby modes available with this device.

The selected wireless transceiver was the nRF2401 form Nordic Semiconductor [20]. This is a single-chip radio transceiver for the world wide 2.4 - 2.5 GHz ISM band with a small package size of 5 × 5 × 0.7 mm. This transceiver features embedded protocol software to minimise power consumption and maximise data throughput using its Shockburst® feature.

The chosen antenna for the application was a dielectrically-loaded chip type [21]. The available form factor of 6.5 × 2.2 ×1mm as well as the favourable electrical and radiation characteristics made it the most suitable commercial antenna for the WIMU application. These antennas use low temperature, co-fired ceramic (LTCC) technology to allow the antenna size to be minimized. The electrical specifications include a 50Ω characteristic impedance, omni-directional radiation pattern, greater than unity gain, linear polarization, and a usable bandwidth of 180MHz in the 2.45GHz ISM band.

D. RF Subsystem

Having described the various system components, the RF subsystem is now described in more detail. In particular, the interface between the radio transceiver and antenna (or balun circuit) is described. The balun is a key component in balanced circuit topologies, typical of modern radio transceiver architectures. The term balun is an abbreviation of the words *balance* and *unbalance* and is defined as a device that converts a balanced system such as a two-conductor line to an unbalanced coaxial line

[22]. The balun plays an important role in maximizing radio communications performance while minimizing power consumption.

To explain the need for a balun, Figure 7 shows two cases in which a balanced dipole antenna is driven firstly by a balanced line and secondly via an unbalanced line.

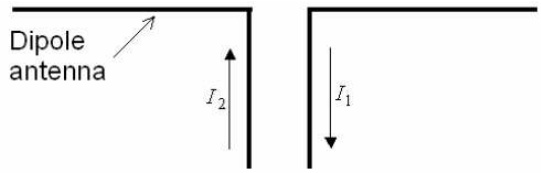

(a) Balanced connection

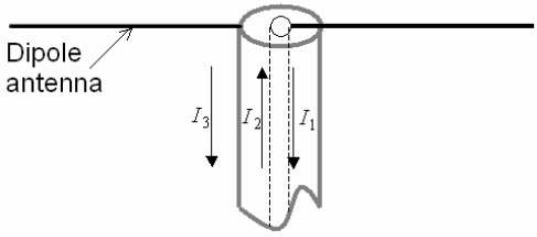

(b) Unbalanced connection

Figure. 7: Balanced dipole connected to (a) Balanced line, (b) Unbalanced line.

In Figure 7(a), a current I_2 flows on the left conductor of the balanced line into the left leg of the dipole antenna while an equal but opposite current I_1 returns on the right conductor. Since both the currents are equal and opposite on the line, there is a net cancellation of currents on the line. In Figure 7(b), the balanced transmission line is replaced with a coaxial line. In this case, the currents I_1 and I_2 cancel each other within the line. However, since current I_1 cannot penetrate beyond the shield, a net current I_3 flows on the outer shield. The consequences are that the current in the shield becomes, undesirably, part of the radiating system and give rise to unwanted radiation from the line itself. The presence of this radiation from the line modifies the radiation pattern of the antenna and affects the impedance of the antenna. A balun is

therefore required to suppress the unwanted current on the outer conductor of the unbalanced line.

Baluns are commonly realized by using either of three types of circuit elements: discrete transformers, transmission lines, or lumped element components [22-24]. Traditionally, baluns operating at microwave frequencies are designed using distributed topologies. However, at frequencies used for wireless sensor nodes such as the 2.45 GHz ISM band frequencies, distributed designs tend to be large and consume a large area on the printed circuit board. For highly miniaturized wireless nodes, lumped-element designs, consisting of discrete inductors, capacitors, and resistors are popular due to the small size possible when SMT components are used. The balun implementation for this application is shown in Figure 8.

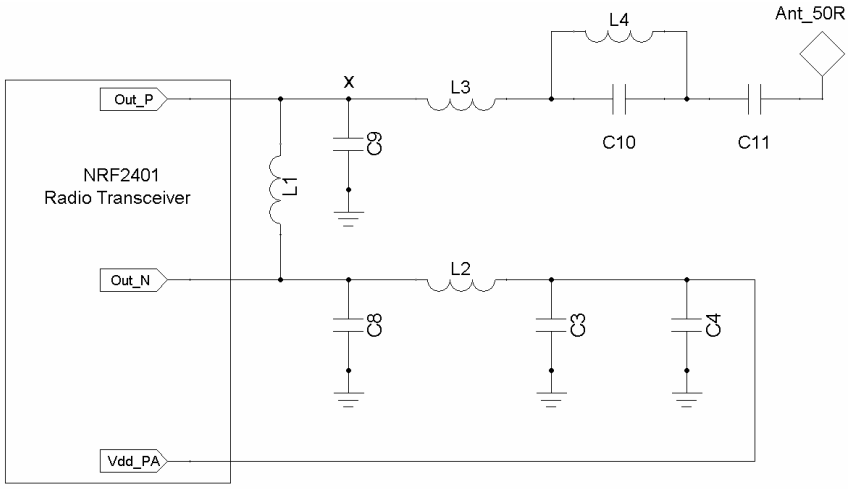

Figure. 8: nrf2401 Balun and Matching Circuit

The balun has four different tasks:

- Implement a balun function by transforming the balanced transceiver signals (denoted *Out_P* and *Out_N* in Figure 8) to balanced antenna signal (denoted Ant_50R).

- Transform the output impedance of the radio ($100 - j175\Omega$) to an impedance of 50Ω for the antenna.
- Suppress the level of transmitter output harmonics to meet the required radio emission regulations.
- Suppress local oscillator (LO) signal leakage in receive mode.

For the balun shown in Figure 8, at the centre frequency of 2.45 GHz, the differential output signals *Out_P* and *Out_N* combine in phase at node x, thus performing the required balun function. The impedance transformation between the transceiver and antenna is performed via components L3 and C10 with an inductor L4 included to form a LO trap. Capacitors C8 and C9 are used for harmonic suppression with capacitor C11 used for DC blocking. Additional LO leakage suppression is performed via components L2 and C3 and the Vdd_PA signal is filtered via capacitor C8. It is important to note that all practical components have parasitics that are affected by component placement. It is difficult to calculate the ideal component values and complex simulation models are required. A methodology has been developed that has been applied to the optimization of this circuit and is described in [25].

E. Power Subsystem

For this application, the WIMU is intended to be battery powered and as mentioned previously, the node needs to be power aware and keeping current consumption to a minimum is critical in order to maximize battery life. The power distribution circuitry has been designed to allow various circuit elements to be switched off under software control. Using this scheme, the microcontroller is powered continuously but in order to save power, it can be programmed to enter sleep mode or standby mode. The

regulators were chosen to have enable signals under microcontroller control. Table 1 summarizes the power control functions of the main subsystem elements.

TABLE 1

Power control signals

Device	**Power Control**
Gyros	YES
Micro	NO
Accelerometers	YES
Radio	YES

F. Interconnect Design

The first step in specifying the interconnect subsystem was to determine the number of PCB layers or layer stackup needed to successfully implement the design. Ideally, a solid ground and supply plane would be required to provide a low-impedance power distribution system for the sensitive analog sensor electronics as well as the noisier digital electronics. A good deal of time was spend in performing trial PCB layouts of the design and it was determined that the design could be implemented using a two-layer stackup. Another factor that was considered at this time was the types of commercial flex material available and the required design rules for these types of materials. In consultation with various flex manufacturers, it was determined that utilizing a four or six layer stackup would mean that it would be extremely difficult to bend the substrate with a small radius of curvature, even for the thinnest flex material available. It was determined that a 90 degrees bend would be possible with a 4-layer stackup but with a much larger bend radius of greater than 1mm. This was found to be unacceptable as such a large radius of curvature would add a further 2mm to the outer dimensions of the folded cube and would add gaps along each folded edge, leading to a larger and weaker structure. After careful analysis, it was concluded that a 2-layer stackup would be sufficient.

In order to realize a WIMU in a small cube structure, the choice of materials would be critical. A good deal of experience had already been gained from previous work using commercial thin-film flexible polyimide substrate [13, 15, and 16]. Here, a 3-D module consisting of a thin, flexible polyimide substrate with folded flex was fabricated and tested. This work showed that folded flex provides a very good potential solution to the system packaging challenges inherent in implementing functional miniaturised sensor modules. For this particular implementation, the flex material would need to be flexible enough to allow a 90-degree fold to be made at the bend planes in order realize a cubic structure while at the same time ensuring that the flex substrate would not tear or crack. In addition, the substrate would need to have a certain degree of rigidity to ensure that after folding, the cube shape would be maintained before final assembly and packaging.

For this work, a commercial flex material AP-8525 from DuPont™ [26] was investigated. This is a flexible, double-sided, all-polyimide copper clad material and has a good balance of electrical and mechanical properties especially bend and crease performance that is important for this application. In addition, the material has excellent thermal resistance, unique thick-core product for controlled impedance and excellent dielectric thickness tolerance/electrical performance, all of which are very important properties for this RF application. Some of the key material properties for the flex material are summarized in Table 2.

TABLE 2

AP8525R Material Properties

Dielectric Thickness	18um
Copper Thickness	50um
Dielectric Constant at 2.45 GHz	3.3
Loss Tangent at 2.45 GHz	0.003

In terms of choosing an appropriate soldermask material, conventional soldermask is not suitable due to its rigidity and tends to crack during bending.

Therefore for this application, a flexible soldermask or "coverlay" was investigated used to ensure that the board could be bent without cracking. In particular, a Pyralux, LF0110 coverlay composite material [27] was recommended by the PCB manufacturer. This material is a flexible substrate with an adhesive backing that is applied to the surface of the flex circuit to provide environmental and electrical insulation and some of the main properties are listed in Table 3.

TABLE 3
LF0110 Coverlay Material Properties

Adhesive Thickness	25um
Kapton Thickness	25um
Dielectric Constant at 1 MHz	4
Loss Tangent at 1 MHz	0.03

A flexible solder resist NPR-80 [28] was chosen designed to prevent solder bridges during soldering. In order to pattern the coverlay and soldermask, conventional lithography was discussed with the PCB manufacturer but it was determined that laser ablation is a better alternative to traditional lithography. In particular, laser ablation is easier to use on flexible substrates and produces more accurate features. Having determined the best flexible materials and manufacturing process for this application a decision was made to choose the manufacturer that could best meet the PCB layout design rules. One of the key design goals with respect to manufacturing was guaranteeing the reliability of the FPC once a 90 degree bend had been created. Some useful guidelines were provided by the chosen FPC manufacturer in order to meet this goal.

- Build prototype system using an initial test substrate to allow characterization of the material for the application and then refine for final system.
- The copper laminate thickness should be kept to a minimum.
- Use top and bottom-side coverlay braces at the bend planes to reduce the risk of interconnect failure during folding.
- Only plate pad locations to minimize trace copper thickness and increase flexibility.
- Pre-crease circuits at bend planes to encourage the circuit to bend at the desired point.
- Evaluate Nickel Gold finish for prototype and replace as necessary

SYSTEM FABRICATION

A. Prototype Material Specification

Following the manufacturer's guidelines, a prototype flex circuit was first specified, with the decision made to place additional coverlay strips at the bend planes as shown in Figure 9 to increase the strength of the substrate during bending. Table 4 shows a summary of the stackup and materials used.

TABLE 4
Stackup and materials for the prototype system

Prototype Build		
Material	**Layer**	**Thickness (um)**
Soldermask	Nippon NPR-80 Flexible Solder resist	50
Coverlay	LF0110 Coverlay	50
Substrate	AP8525R Copper Clad Flex	85
Coverlay	LF0110 Coverlay	50
Soldermask	Nippon NPR-80 Flexible Solder resist	50
Total Thickness		**285**

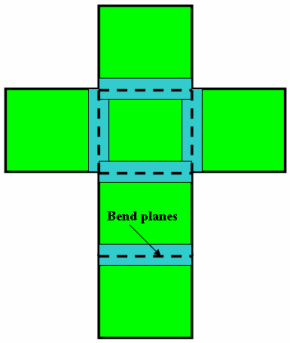

Figure. 9: Plan view of the FPC substrate for the prototype system

C. Prototype System Fabrication & Failure Analysis

The prototype flexible printed circuit was fabricated and the top and bottom surfaces of the finished substrate are shown in Figure 10(a).

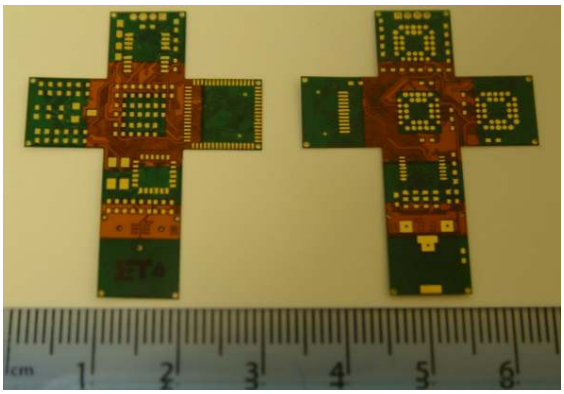

(a)

(b)

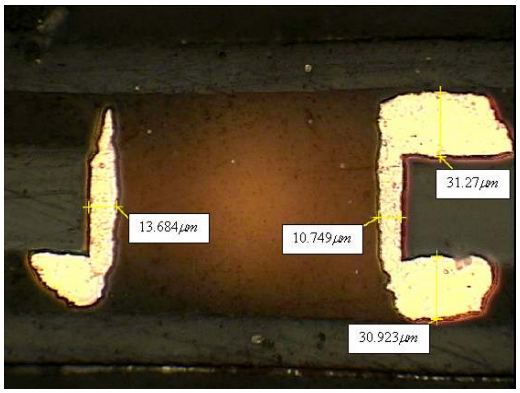

(c)

Figure.10: (a) Fabricated substrate, (b, c) VIA manufacturing defects

On closer inspection, the manufactured plated-through-hole (PTH) via quality was discovered to be a problem as shown in Figure 10 (b). A microsection analysis shown in Figure 10(c) confirm that breakout of the PTH vias had occurred. This was later identified to be caused by the manufacturer having drilled the holes too large. It can be seen that in some areas, the PTH vias had a minimum of approximately 8 microns of copper down the PTHs which was also identified as a reliability concern.

In addition to the above manufacturing defects, a bend test was performed on the prototype flex. In order to allow the subsequent folding of the substrate in an accurate and controlled manner, a dedicated test jig was designed specifically for this purpose. Figure 11 shows the final jig of brass construction, with an accurately milled cut-away to allow placement of the delicate substrate prior to bending.

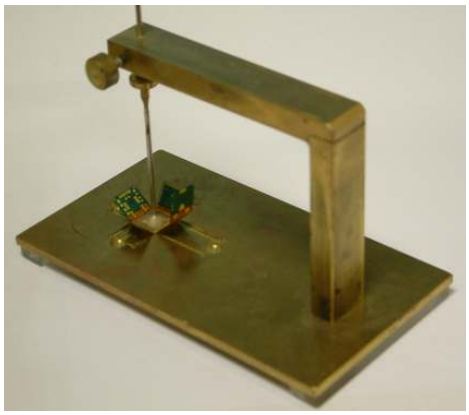

Figure.11: Bending Jig used to crease substrate

Once the substrate was placed, the individual faces could then be accurately creased by carefully applying pressure at the bend plane with a beveled tool. A number of issues were identified post bending. Figure 12 shows cracking of the soldermask and metal close to one of the bend planes, just to the left of the coverlay material.

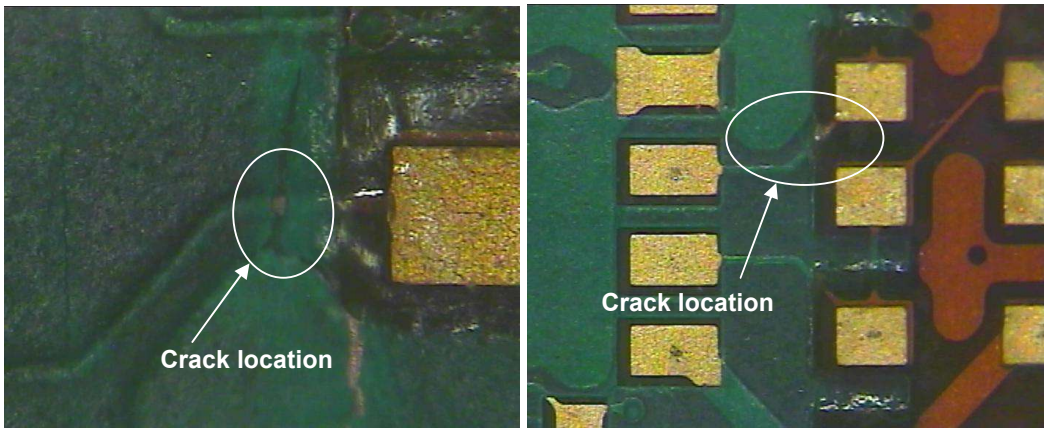

Figure.12: Soldermask cracking

This was investigated further and was attributed to the presence of a large area of copper on the associated bend plane. This copper area was included to provide a good RF return path between the radio transceiver and antenna. The effect of the copper during bending was to move the stress at the bend plane further to the left towards the balun components and this would need to be addressed in the final system. In addition to the above tests on the unpopulated FPC circuit, a number of tests were also carried out on the populated FPC substrate shown in Figure 13.

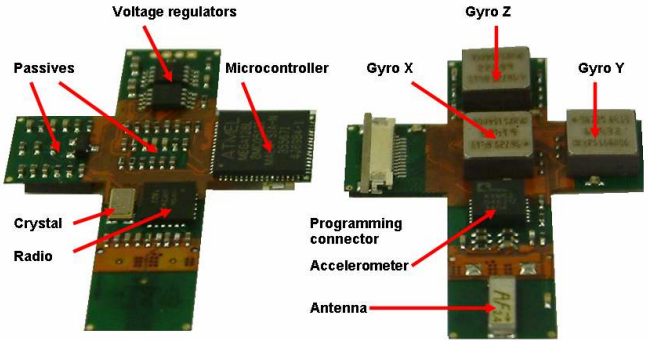

Figure.13: Populated FPC substrate

Initial functional tests were performed by programming the WIMU modules in planar form. Then, having bent the substrate into a cube, an additional issue was observed in relation to the performance of the gyroscopes. This problem was eventually traced to

buckling of the substrate at the corners of the centre face with open circuits forming on the BGA gyroscope pins devices after bending as shown in Figure 14.

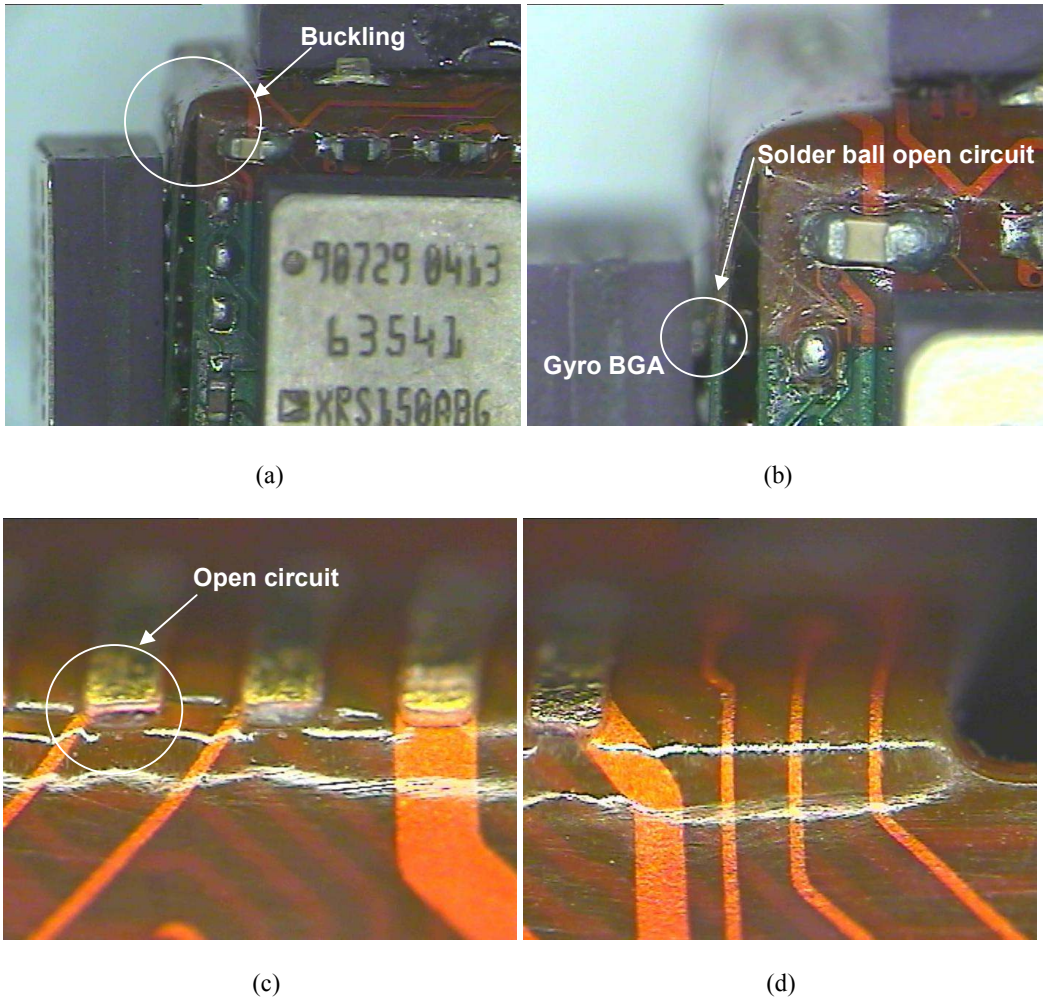

Figure.14: (a) Corner buckling, (b) BGA Open circuits,
(c) Bend plane open circuits, (d) Reliable bend plane interconnect

The bend planes on the centre face were surrounded by strips of additional coverlay material and it was determined experimentally that these areas were the most difficult to bend. In addition, open circuits were observed in areas where component pads were placed near the bend plane as in Figure 14(c). This problem manifested itself on the traces with minimum width (137um) and did not occur on the wider traces or traces that did not have coverlay apertures in the coverlay as in Figure 14(d). This effect was also seen in a previous work [13] where coverlay openings on the bend plane

exhibited a degree of metal cracking after bending. Of six circuits that were fabricated and tested, five failed during bending, resulting in a failure rate of approximately 83%. Obviously, this failure rate and unreliability is unacceptable for the final implementation. Having identified a number of serious issues with the prototype flex circuit, a number of corrective steps were identified for the final circuit implementation as follows:

- Minimize the total thickness of FPC materials and use an alternate, more flexible metallization finish to Nickel-Gold.
- Eliminate use of coverlay at bend planes and instead use a thin flexible soldermask for the entire flex circuit.
- Eliminate copper areas overlapping at bend planes.
- Include 1mm holes at all bend planes to avoid creasing/buckling at corners.
- Widen all pad entry traces close to the bend plane to reduce risk of open circuits.
- Pre-fix BGA devices prior to bending.

The new stackup and materials for the final build are shown in Table 5 and the total thickness is reduced by approximately 72% by using a much thinner starting flex material [29].

TABLE 5
Stackup and materials for final system

Final Build		
Material	**Layer**	**Thickness (um)**
Flexible Soldermask	Nippon NPR 80	10
Substrate	Toray Copper Clad Flex	88
Flexible Soldermask	Nippon NPR 80	10
Total Thickness		**108**

The finish for this build was also specified on this occasion as an immersion tin finish which is more flexible than the previous finish of Nickel-Gold. Figure 15(a) shows a cross-section of a PTH via for the finished substrate. PTH via formation is very much improved compared to the previous revision, with a well defined annular ring for the pads. In addition, the improved deposition of copper (minimum of approximately 20um copper) for the via side walls leads to much improved interconnect reliability.

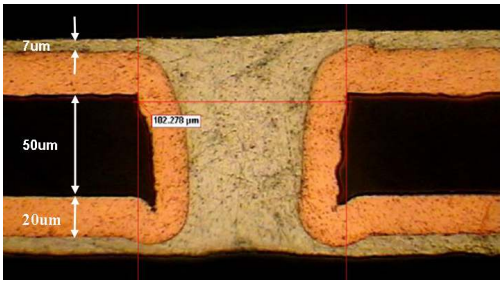

(a)

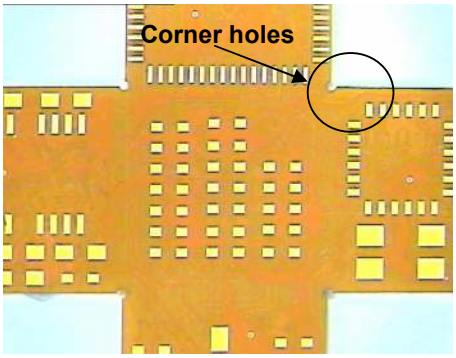

(b)

Figure.15: (a) Reliable PTH via process, (b) Corner holes to facilitate improved bending

In order to characterize the new material, the previous bend tests were repeated and it was found that the new material did not have the same issues that were evident in the original tests. The addition of the small holes at the corners shown in Figure 15(b) reduced the bending stresses, particularly on the centre face and the removal of the copper at the bend plane between antenna and radio transceiver eliminated the trace cracking problems. Based on the positive results obtained, the thinner flex material was chosen for the final fabrication of the WIMU.

B. Final System Fabrication & Failure Analysis

Prior to population of the final flex circuit, a bend was formed on each bend plane and then bent back in the opposite direction. This left a flat crease along each bend plane, making it easier to fold the circuit once populated.

The pre-creased PCBs were populated with components and the final planar PCB assemblies are shown in Figure 16(a). In this configuration, the assembly was programmed and tested prior to folding into a cube form factor. Once tested, the gyroscopes were secured with epoxy prior to bending to avoid the risk of the BGA gyro pins lifting and causing open circuits after folding. The assemblies were then folded and once the cube shape was formed, the adjacent edges of the cube were fastened to each other using an epoxy resin. The final folded cube is shown in Figure 16(b).

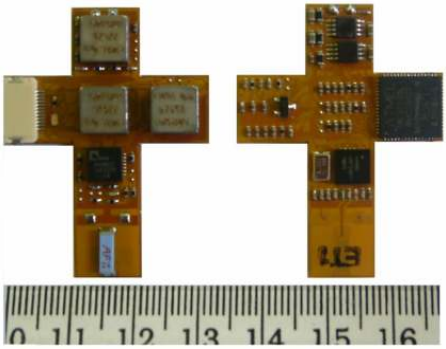

(a)

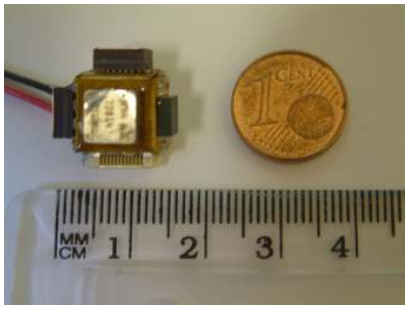

(b)

Figure.16: Final flex circuit, (a) Planar assembly, (b) Folded WIMU assembly next to a 1-cent coin

Of the 10 final WIMU systems that were characterized and tested with the new substrate material, a significant improvement was observed with no failures being recorded after folding the flex into a 3D cube.

APPLICATION DEVELOPMENT

A. Software Development

The embedded software on the WIMU transmitter and receiver are now described. The transmitter software consists of various functions that perform a number of tasks in order for capture of the gyro and accelerometer measurement data and the wireless transmission of this sensor data. The radio transmits each byte of data on a chosen channel (1) of the available ISM bandwidth between 2.4 and 2.48 GHz. On the receiver side, the embedded software on the WIMU receiver consists of various functions that capture the transmitted gyro and accelerometer measurement data from the WIMU transmitter. A user-friendly graphical user interface was developed using Labview in order to display the captured motion data from the WIMU transmitter. An example of the GUI output screen is shown in Figure 17, displaying the measured gyroscope and accelerometer outputs in real time when the WIMU unit is moved.

B. System calibration and test

Since the WIMU module has been developed using off the shelf components, the performance of the module had to be tested for basic functionality and then for the generation of a set of system specifications. A number of experiments were designed and executed to carry out this characterization. The system was connected to a PC wirelessly to log the information received from the WIMU for off board analysis. Each of the sensors was subject to conditions that excited the respective sensing properties (tilt, rotation etc) and the results were recorded and compared to the

manufacturers' specifications. The accelerometers were subject to tilt extremes to measure the max, min and zero offsets. The gyroscopes were excited using a calibrated rotating table. All of the data was recorded and analyzed used a customized Labview application. As described previously, the Labview GUI application was developed to provide a visual analysis of the sensor data being produced by the WIMU. This application allowed for the viewing of the sensor signals in real time and contained integrated calibration routines that allowed for the calculation of the resolution of each the sensors.

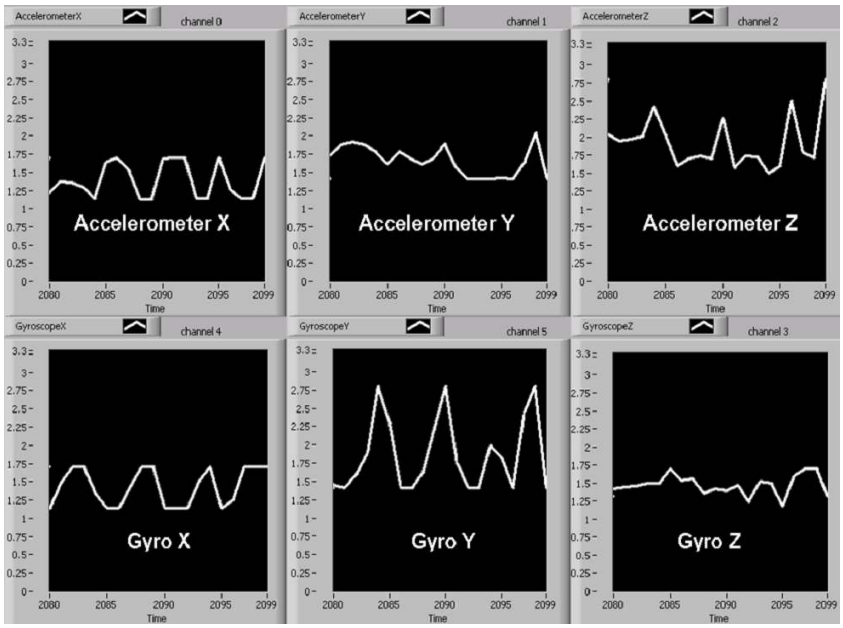

Figure.17: Labview GUI for the WIMU application

In order to ensure that the WIMU is calibrated properly the voltage offset, sensitivity and non-orthogonality of the gyroscopes and accelerometers need to be evaluated so their effects can be mitigated during performing measurements. In addition, for accurate calibration, the mutual misalignment of the sensors to each other needs to be determined. However, determining the errors due to sensor non-orthogonality and mutual misalignment requires complex mathematical methods that are not treated

here. In this work, a relatively simple calibration method for estimating offset and sensitivities is used while the non-orthogonality and alignment issues will be the aim of future work. For calibration, measurements made directly from the IMU are referenced with respect to the three defined IMU sensors axes as shown in Figure 18.

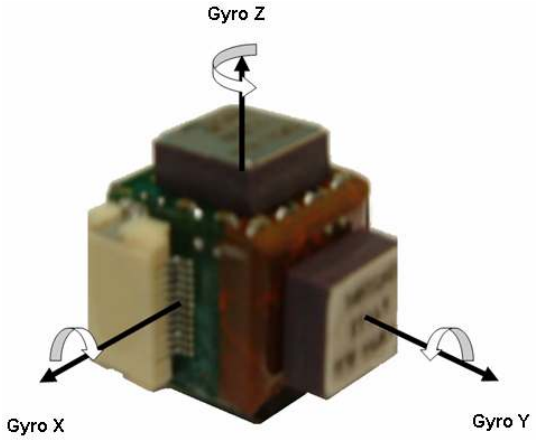

Figure.18: WIMU gyro & accelerometer reference frames

In order to characterize the accelerometer offsets and sensitivities, it is required to know the maximum and minimum values of acceleration when the accelerometer is oriented in two specific configurations. The first of these configurations is with the accelerometer held stationary and one of its three axes pointing towards the earth's core. In this case, the sensor output will be a maximum while experiencing a force of 1g or 9.81m/s^2 and the sensor output voltage is denoted here by the value *VMax*. The second configuration is with the accelerometer's sensor axis perpendicular to the earth's surface but pointing away from the earth's core. In this configuration, the sensor output will be a minimum, denoted by the value *VMin*.

The measured acceleration offset is then given by equation 1 where

$$A_{offset} = \frac{VMax + VMin}{2}(Volts)\,. \tag{1}$$

The measured accelerometer sensitivity is given by equation 2 where

$$A_{sensitivity} = \frac{V\max - V\min}{2}(Volts/g) \ . \qquad (2)$$

In order to estimate the voltage offset of the gyroscopes, it is necessary to rotate the WIMU about the three principal axes and then calculate the average gyroscope output for each orientation. The estimation of the gyroscopes sensitivities was carried out using a digital turntable. The WIMU module was placed on the turntable ensuring the table's axis of rotation was in line with the sensor's sensitive axis (Note that the angular velocity will be the same for all distances from the turntable's centre). The table was set to a nominal angular velocity of 20 revolutions per minute. The received data was logged and an example of the gyroscope X-axis output from this calibration is shown in Figure 19.

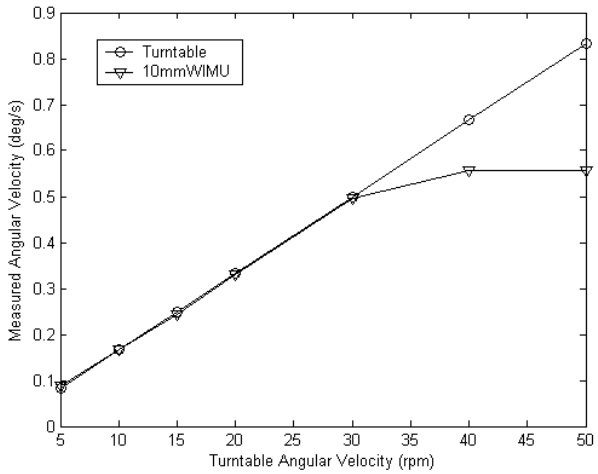

Figure.19: Measured WIMU X-axis gyro response

The measured angular velocity is very accurate for angular velocities less than 30rpm and is limited by the sensitivity of the gyro. This is not an issue though as the sensitivity of the gyro is easily changed by adjusting the value of a single resistor,

depending on the application. The complete characterization and calibration measurements are summarized in Table 6.

TABLE.6

Summary of WIMU calibration measurements

Orientation	Parameter	Calibrated Value
X	Accelerometer offset	1.52 V
	Accelerometer sensitivity	0.6336 V/g
	Gyroscope offset	1.49 V
	Gyroscope sensitivity	0.056 V/degree/sec
Y	Accelerometer offset	1.48 V
	Accelerometer sensitivity	0.6464 V/g
	Gyroscope offset	1.5 V
	Gyroscope sensitivity	0.054 V/degree/sec
Z	Accelerometer offset	1.5 V
	Accelerometer sensitivity	0.669 V/g
	Gyroscope offset	1.48 V
	Gyroscope sensitivity	0.055 V/degree/sec

The measured calibration constants for each sensor were then incorporated into the WIMU firmware and GUI application to ensure the accuracy of subsequent system measurements.

C. RF Testing

Some simple tests were carried out in order to test the RF communications range of the WIMU. The antenna performance was tested in an open-field environment, free from nearby obstructions that could affect the accuracy of the measurements. The transmitting mote was configured to send 100 packets of data for subsequent reception by the receiving mote. The transmitter and receiver motes were each mounted on a wooden pillar to a height of 1.5m. The packet loss was then measured as a function of distance by varying the horizontal separation between the transmitting and receiving motes. This was accomplished by moving the transmitter while leaving the receiver stationary and measuring the packet loss for each measurement. A laptop was connected to the receiving mote via an RS232 cable in order to capture and display the results that are shown in Figure 20.

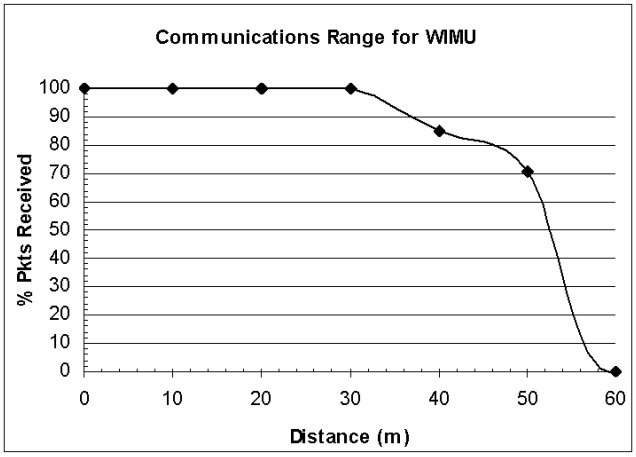

Figure.20: Packet Loss Measurements

It can be seen that the WIMU system has a range of 60m approximately in open-air. The module was tested indoors and the range fell to 20m approximately in a typical LAB-corridor environment. This is expected and is attributed to the multi-path fading effects that are experienced in non-ideal RF indoor environments.

CONCLUSIONS

In this paper, a highly miniaturized wireless inertial measurement unit has been designed and fabricated using a thin-film flexible substrate and employing a novel 3D packaging technique. Using this technique, a 78.5% saving in volume was obtained in decreasing the module size from a 25mm to a 15mm cubed.

For the initial system prototype, the reliability was extremely poor with only a 16% pass rate after folding the flex from a planar cross to a cube shape. The causes for these failures were investigated in detail and a number of corrective measures were taken to solve these problems for the final system implementation. The main issue identified for the prototype system was the consistent failure of the interconnect in several specific locations close to the bend planes, caused mainly by lack of substrate flexibility in these critical areas. Another effect observed was the buckling at the corners of the centre flex face and the spreading of stress from the bend planes to nearby interconnect. In addition, the apertures for component pads close to the bend planes led to increased stress in these areas with failure of traces with minimum line width. Another issue identified was the formation of open circuits on the gyroscope ball-grid-array pins, again caused by lack of flexibility of the substrate.

The above issues were successfully resolved by carefully specifying the properties of the flex material as well as tailoring the mechanical aspects of the design to reduce bending stress and increase strength at key locations. The result is that from the final quantity of ten boards that were fabricated and populated, there were no failures on the final system revision.

Acknowledgments

We would like to greatly acknowledge the support of Enterprise Ireland for the funding of this work under the Proof-Of-Concept project PC/2005/229.

REFERENCES

[1] Barbour, N and Schmidt, G. (2001), “Inertial sensor technology trends”, IEEE Sensors Journal, pp. 332–339.

[2] Varadan, V.K., Varadan, V.V., Subramanian, H. (2001), “Fabrication, characterization and testing of wireless MEMS-IDT based microaccelerometers”, Sensors and Actuators, A: Physical, 90 (1-2), pp. 7-19.

[3] King, K., S. W. Yoon, et al. (2008). "Wireless MEMS inertial sensor system for golf swing dynamics" Sensors and Actuators A: Physical 141(2): 619-630.

[4] Farella, E., Pieracci, A., Benini, L., Acquaviva, A. (2006), “A wireless body area sensor network for posture detection”, Proceedings - International Symposium on Computers and Communications, art. no. 1691069, pp. 454-459.

[5] Farella, E., Pieracci, A., Benini, L., Rocchi, L., Acquaviva, A. (2008), “Interfacing human and computer with wireless body area sensor networks: The WiMoCA solution”, Multimedia Tools and Applications, 38 (3), pp. 337-363.

[6] Lynch, A., Majeed, B., O'Flynn, B., Barton, J., Murphy, F., Delaney, K., O'Mathuna, S.C. (2005), “A wireless inertial Measurement system (WIMS) for an interactive dance environment”, Journal of Physics: Conference Series, 15 (1), pp. 95-100.

[7] Bandala, M. and Joyce, M.J. (2008), “Tracking of internal organ motion with a six degree-of-freedom MEMS sensor: Concept and simulation study”, Measurement Science and Technology, 19 (2), art. no. 024006.

[8] Bandala, M. AND Joyce, M. (2007), “Wireless inertial sensor for tumour motion tracking”, Journal of Physics: Conference Series, 76 (1), art. no. 012036.

[9] Van Acht, V., Bongers, E., Lambert, N., Verberne, R. (2007), “Miniature wireless inertial sensor for measuring human motions”, 29th Annual International Conference of IEEE-EMBS, Engineering in Medicine and Biology Society, EMBC'07, art. no. 4353790, pp. 6278-6281.

[10] Microstrain Microminiature Sensors, (2008), GLink® Wireless Accelerometer product documentation. Available at http://www.microstrain.com/g-link.aspx

[11] XSens Motion Technologies, (2008), Xsens product documentation, Available at http://www.xsens.com/en/products/human_motion/xbus_kit.php

[12] Barton, J. et al, "Miniaturised Inertial Measurement Units (IMU) for Wireless Sensor Networks and Novel Display Interfaces", (2005), Proc. ECTC, Lake Buena Vista, Florida, May 31- June 3, pp 1402-1406.

[13] Barton, J., Gonzalez, A., Buckley, J., O’Flynn, B., O’Mathuna, S.C., (2007), “Design, Fabrication and Testing of Miniaturised Wireless Inertial Measurement Units”, Proc. ECTC 2007, Reno, Nevada, USA, May 29 -June 1, pp 1143-1148.

[14] O'Flynn, B. et al, (2005), "A 3-D Miniaturised Programmable Transceiver", Microelectronics International, Volume 22, Number 2, (2005), pp. 8-12.

[15] Majeed, B., Van Jans, J.-B.S., Paul, I., Barton, J., Mathuna, S.C.O., Delaney, K. (2005), Material characterisation and process development for miniaturised wireless sensor network module”, PhD Research in Microelectronics and Electronics – Proceedings of the Conference, I, art. no. 1543047, pp. 211-214

[16] Majeed, B., Delaney, K., Barton, J., McCarthy, N., O'Mathuna, S.C., Alderman, J. (2006), "Fabrication and characterization of flexible substrates for use in the development of miniaturized wireless sensor network modules", Journal of Electronic Packaging, Transactions of the ASME, 128 (3), pp. 151-158.

[17] ADXRS150 ±150°/s Single MEMs Chip Yaw Rate Gyro, Available from http://www.analog.com/

[18] KXM52 Analog Accelerometers / Inclinometer, Available from http://www.kionix.com/

[19] ATMega128L High-performance, Low-power AVR® 8-bit Microcontroller, Available from http://www.atmel.com/

[20] NRF2401A ultra-low power 2.4GHz transceiver, Available from http://www.nordicsemi.com/

[21] ANT-2.45-CHP, 2.45GHz ¼-wave monopole chip antenna, Available from http://www.antennafactor.com

[22] C. A. Balanis, "Antenna Theory: Analysis and Design," Second Edition, John Wiley & Sons, Inc., New York, 1997.

[23] T. Lee, "The Design of CMOS Radio-Frequency Integrated Circuits", Cambridge University Press, New York, NY, 1998.

[24] Bakalski, W., Simbiirger, W., Kehrer, D., Wohlmuth, H. -D., Rest, M., and Scholtz, A.L., (2002), "A monolithic 2.45GHz, 0.56 W power amplifier with 45% PAE at 2.4V in standard 25GHz ft Si-bipolar,'' in Proceedings of IEEE International Symposium on Circuits and Systems, Scottsdale, Arizona, May 26-29, pp. 117—119.

[25] Buckley, J., O'Flynn, B., Popovici, E., O'Mathuna, S.C., (2007), "Design and Optimization of a Lumped-Element Balun for a Zigbee Wireless Sensor Node", CIICT, China Ireland International Conference on Information and Communications Technologies, Dublin, Ireland August 28th and 29th, pp. 211-214

[26] AP-8525R, Pyralux® AP, All-Polyimide Flexible Laminate, Available from http://www.dupont.com

[27] LF0110 Flexible Composite Coverlay, Available from http://www.dupont.com

[28] NPR-80 photo-image solder resist, Available from http://www.nptcorp.com

[29] Toray 04-50-04, Copper clad film, Available from http://www.toray.co.jp